Increasing Sequence Length Favors α-Helix over 3_{10}-Helix in Alanine-Based Peptides: Evidence for a Length-Dependent Structural Transition†

Wayne R. Fiori, Siobhan M. Miick,‡ and Glenn L. Millhauser*

Department of Chemistry and Biochemistry, University of California, Santa Cruz, California 95064

Received August 2, 1993; Revised Manuscript Received September 20, 1993®

ABSTRACT: Ala-based peptides form marginally stable helices at low temperature and are conventionally considered as mixtures of α-helix and random coil. However, recent work with doubly spin-labeled peptides suggests that short 16-residue sequences contain a significant fraction of 3_{10}-helix near the N-terminus (positions 4–8). Using the same double-label strategy, we report on the helix geometry of the peptides Ac-$(AAAAK)_n$A-NH_2 with $n = 3$ and $n = 4$. The 16-mer ($n = 3$) is now examined at a region near the C-terminus, and there is evidence for 3_{10}-helix here as well. The 21-mer ($n = 4$) is examined in three regions of the sequence. In dramatic contrast to the 16-mer, the 21-mer exhibits the signature of α-helix at the N-terminus and on through the middle of the peptide. The 21-mer C-terminus, however, adopts the 3_{10}-helix geometry as is often found for C-termini in protein α-helices. These data indicate that the proportion of α-helix and 3_{10}-helix in Ala-based peptides depends upon the sequence length.

Helical peptides have emerged as model systems for exploring principles of secondary structure in proteins [e.g., Marqusee et al. (1989), Lyu et al. (1990), Kemp et al. (1991), Mertuka et al. (1991), Creamer and Rose (1992), Scholtz and Baldwin (1992), and Vila et al. (1992)]. Therefore, it is extremely important to determine the detailed geometry of these peptides. Until recently most experimental evidence indicated that helix-forming peptides constructed from the common (C_α-monosubstituted) amino acids would exclusively adopt the conformation of an α-helix when in aqueous solution. However, recent work using double-label electron spin resonance (ESR) has suggested that short alanine (Ala) 16-mer peptides may actually exist as 3_{10}-helices or as a mixture of α and 3_{10} (Miick et al., 1992).

The geometry of an α-helix is characterized by $i \rightarrow i+4$ hydrogen bonding whereas the more highly pitched 3_{10}-helix has $i \rightarrow i+3$ bonding. α-Helices are more common than 3_{10}-helices in proteins; however, the occurrence of 3_{10}-helices is not rare (Barlow & Thornton, 1988). They are routinely found at the ends of α-helices and also between β-strands in all-β proteins. The existence of 3_{10}-helix geometry in peptides is less clear. NMR experiments on helical peptides often reveal connectivities consistent with a coexistence of α-helix and 3_{10}-helix, but the conclusions are usually tentative [e.g., Osterhout et al. (1989)]. A notable exception to this is a recent study on the Ala-based 21-mer with eight sequential Ala's at the N-terminus. Analysis of the NOEs showed that the first four residues (positions 1–4) could be clearly mapped to α-helix (Lockhart & Kim, 1993).

The achiral $C_{\alpha,\alpha}$-disubstituted residue α-aminoisobutyric acid (Aib) readily forms 3_{10}-helices. Crystallographic studies have shown that poly(Aib) retains the 3_{10}-helix conformation regardless of peptide length (Toniolo & Benedetti, 1991). Interestingly, the mixed sequence $(Aib\text{-}L\text{-}Ala)_n$ exists as 3_{10}-helix for $n = 3$ and mixed $\alpha/3_{10}$-helix for $n = 4$, thereby demonstrating a length-dependent $3_{10} \rightarrow \alpha$ transition in Aib-rich peptides (Pavone et al., 1990). The nature of 3_{10}-helix vs α-helix content in Ala-based peptides of increasing length is as yet unexplored and is the subject of this paper.

In past work we combined circular dichroism (CD) with double-label ESR to determine the conformation of a 16-mer peptide (Miick et al., 1992). CD indicates the total helix content within a peptide. Double-label ESR provides information on the relative average distances, $d(i,j)$, between labeled side chains. The length scale for the interaction between nitroxide spins is longer than that for NMR NOEs, and this provides a unique view of helix structure. α-Helix and 3_{10}-helix are distinguished mainly by the relative spacing between side chains $i \rightarrow i+3$ and $i \rightarrow i+4$ residues apart in the peptide sequence (Schulz & Schirmer, 1979). Specifically, α-helix is characterized by $d(i,i+3) \geq d(i,i+4)$ whereas 3_{10}-helix has $d(i,i+3) < d(i,i+4)$. These rankings are readily determined by line-width measurements in the ESR spectra. With the previously reported 16-mer, the helix geometry was mapped between residues 4 and 8, and the interactions between side chains were clearly consistent with 3_{10}-helix.

In view of the length-dependent $3_{10} \rightarrow \alpha$ transition in Aib-based peptides and recent NMR findings, we report here on the position-dependent conformations of both a 16-mer and a 21-mer Ala-based peptide using double-label ESR. Doubly labeled (biradical peptide) analogs of the 16-mer sequence

Ac-AAAAKAAAAKAAAAKA-NH_2 (3K)

and the 21-mer sequence

Ac-AAAAKAAAAKAAAAKAAAAKA-NH_2 (4K)

are examined using the peptides in Table I. Cys (C) residues are introduced to provide site-specific attachment of the MTSSL nitroxide spin label (Berliner et al., 1982; Altenbach et al., 1990; Miick et al., 1991). The 3K-(4,7) and 3K-(4,8) doubly labeled peptides were the subject of a previous publication. Two new 16-mers report on the conformation toward the C-terminus (positions 9–13). The findings reported here show $d(i,i+3) < d(i,i+4)$ in support of 3_{10}-helix content

† This work was supported by grants from the National Institutes of Health (GM46870), the National Science Foundation (DMB8916946), and the Petroleum Research Fund, administered by the American Chemical Society (25227-AC4).

* To whom correspondence should be addressed.

‡ Present address: Department of Molecular Biology, Scripps Research Institute, 10666 N. Torrey Pines Road, La Jolla, CA 92037.

® Abstract published in *Advance ACS Abstracts*, October 15, 1993.

0006-2960/93/0432-11957$04.00/0

throughout the 3K peptide. Remarkably, the 21-mer 4K peptide exhibits a different helical conformation. The N-terminus (positions 4–8) and the center (positions 9–13) show $d(i,i+3) \geq d(i,i+4)$, indicative of α-helix geometry, whereas the C-terminus (positions 14–18) shows 3_{10}-helix. These results demonstrate for the first time that 3_{10}-helix vs α-helix content in Ala-based peptides depends upon peptide length.

MATERIALS AND METHODS

Peptide Synthesis, Purification, and Spin Labeling. The peptides were synthesized by Fmoc solid-phase peptide synthesis on a Rainin PS3 peptide synthesizer as C-terminal amides using a 4-[(2′,4′-dimethoxyphenyl)(Fmoc-amino)-methyl]phenoxy (Rink) resin. The N-terminus was capped with acetic anhydride. The peptides were then cleaved from the resin with a 90% trifluoroacetic acid (TFA)/5% thioanisole/5% anisole mixture or 90% TFA/5% triethylsilane/5% anisole and crystallized from *tert*-butyl methyl ether. Dithiothreitol was added to the samples to eliminate disulfide formation. The peptides were first purified by gel filtration chromatography on a Sephadex G-10 column in 10 mM ammonium acetate, pH 4.7, and then by reversed-phase HPLC with a C18 resin using a gradient of 1%/min from 5% to 45% acetonitrile/H_2O in 0.1% TFA and then dried under vacuum and stored at −10 °C. The peptides were reconstituted in 5 mM MOPS, pH 7.1, and were spin labeled at the cysteine residue by a disulfide linkage with methanethiosulfonate spin label (MTSSL, purchased from Reanal, Hungary) by addition of MTSSL in acetonitrile in a 10-fold excess to a final 5% acetonitrile buffered solution. The reaction mixture was subsequently purified by HPLC to obtain pure spin-labeled peptide. Molecular weights for all the labeled peptides were verified by fast atom bombardment mass spectrometry and agreed with the expected values to within 1 amu. After ESR and CD the samples were rechecked by HPLC to ensure that they contained no unlabeled peptide.

Circular Dichroism. The circular dichroism spectra were acquired under temperature-controlled conditions for each of the peptides in 5 mM MOPS buffer, pH 7.1, at peptide concentrations in the range of 50–150 μM. The measurements were made on an Aviv 60DS spectropolarimeter calibrated with (+)-10-camphorsulfonic acid. The samples contained at least 100 μL of sample in a 0.1-cm path-length cuvette. The peptide concentration was determined by double integration of ESR spectra and comparison to a 1 mM 4-hydroxy-TEMPO standard solution. The peptide concentrations are accurate to 5%.

Electron Spin Resonance. Continuous wave ESR spectra of the spin-labeled peptides were acquired from samples with peptide concentrations of 0.3–1.8 mM in 5 mM MOPS buffer at pH 7.1. The ESR spectra did not vary in the concentration range studied. The measurements were made on a Bruker ESP 380 equipped with a TE_{102} rectangular cavity and operating in the continuous wave mode. The modulation frequency was 100 kHz and the amplitude was 0.19 G. Temperature control was maintained with a Bruker variable temperature accessory, and spectra were gathered over a 100-G scan width.

The spectra in Figure 6 were simulated using eqs 23–26 from Luckhurst and Pedulli (1971). Values for the **g** and **A** tensors of MTSSL have been reported previously (Todd & Millhauser, 1991). The correlation time was 1 ns and zero dipolar coupling was assumed. Inhomogeneous broadening from unresolved MTSSL protons was incorporated by convolution with a 0.9-G Gaussian function.

Table I: Peptide Sequences[a]

3K-(4,7)	Ac-AAACKACAAKAAAAKA-NH_2
3K-(4,8)	Ac-AAACKAACAKAAAAKA-NH_2
3K-(9,12)	Ac-AAAAKAAACKACAAKA-NH_2
3K-(9,13)	Ac-AAAAKAAACKAACAKA-NH_2
4K-(4,7)	Ac-AAACKACAAKAAAAKAAAAKA-NH_2
4K-(4,8)	Ac-AAACKAACAKAAAAKAAAAKA-NH_2
4K-(9,12)	Ac-AAAAKAAACKACAAKAAAAKA-NH_2
4K-(9,13)	Ac-AAAAKAAACKAACAKAAAAKA-NH_2
4K-(14,17)	Ac-AAAAKAAAAKAAACKACAAKA-NH_2
4K-(14,18)	Ac-AAAAKAAAAKAAACKAACAKA-NH_2

[a] Peptide sequences examined in this study are represented with the single-letter amino acid code (Ala, A; Lys, K; Cys, C). The spin labels (MTSSL) are specifically attached at the C residues in each of the sequences.

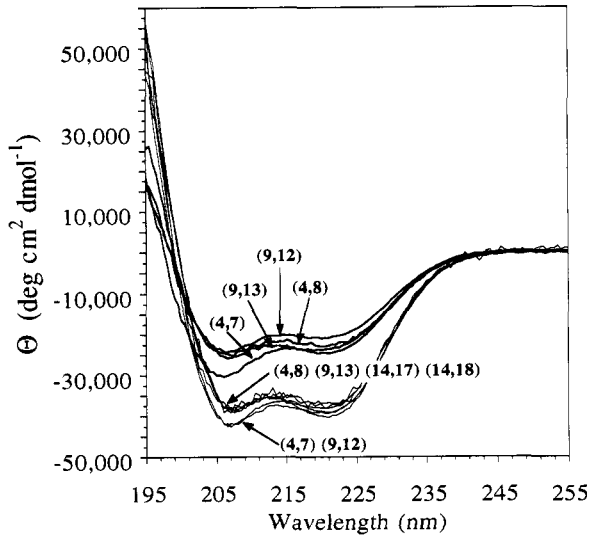

FIGURE 1: Circular dichroism (CD) spectra for the 3K and 4K peptides. All spectra were acquired with sample conditions of 1 °C in 5 mM MOPS bufffer, pH 7.1, at peptide concentrations of 50–150 μM. The 3K peptides are denoted by thick lines and the 4K peptides by thin lines. The double-label positions for each sequence are shown in parentheses.

RESULTS AND DISCUSSION

The CD spectra for all of the doubly labeled peptides (Table I) are shown in Figure 1. The spectra exhibit double minima at 208 and 222 nm characteristic of peptide helices. The mean residue ellipticity at 222 nm is an index of helix content, and the 3K peptides give an average $-[\theta]_{222}$ at 23 000. This is very close to the value of 22 900 reported for the 3K(I) (Marqusee et al., 1989). CD of the 4K peptides indicates that they are more helical than the 3Ks as is expected. The mean for $-[\theta]_{222}$ is 38 000, and this is close to the value of 35 000 reported for a similar 21-residue peptide (Lockhart & Kim, 1993). There are clearly variations among the spectra for the 3Ks as well as the 4Ks of about ±2000 at 222 nm. These variations are reproducible and may represent a CD contribution from the nitroxide side chains. Aromatic side chains absorb in the UV, and recent work has shown that they contribute to the total CD signal when they are located in helical domains of a peptide (Chakrabartty et al., 1993). Similar to aromatic groups, nitroxides also exhibit a strong UV absorbance (λ_{max} = 230 nm; $\epsilon \approx 3000$) (Forester et al., 1968) and may likewise influence the CD spectra. Nevertheless, the variations observed here are small compared to the magnitude of the CD spectra, thereby indicating that the double labels do not significantly influence the peptide helicity.

Figure 2 shows schematically the relative distances between side chains in the two ideal helix conformations. This ranking

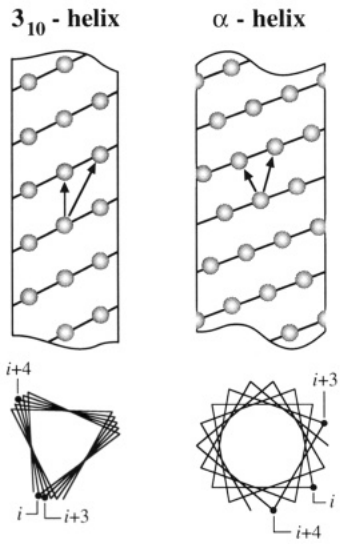

FIGURE 2: Schematic representation of the side-chain interactions in ideal 3_{10}- and α-helices from both side (cylindrical plot) and top (helical wheel) views. The proximity of the $i \rightarrow i+3$ and $i \rightarrow i+4$ side chains are indicated for both helical conformations.

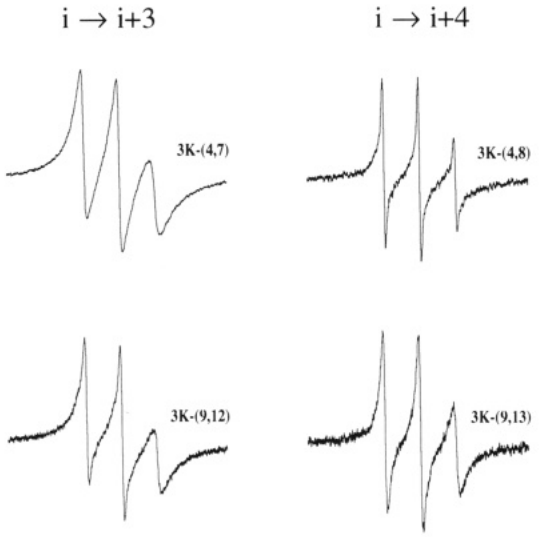

FIGURE 3: Continuous wave ESR spectra (100-G scan) of the 3K double-labeled peptides at 1 °C and peptide concentrations of 0.5–1.8 mM in 5 mM MOPS buffer, pH 7.1. The progression of the spin-label pairs through the helix is from the N-terminus (top spectra) to the C-terminus (bottom spectra).

is based upon distances between side-chain β-carbons and has been verified for doubly labeled peptides with molecular dynamics calculations (Miick et al., 1992). In general, 3_{10}-helix exhibits $d(i,i+3) < d(i,i+4)$ whereas α-helix exhibits $d(i,i+3) \geq d(i,i+4)$. In real protein and peptide helices, there are distortions from ideal helix geometry (Barlow & Thornton, 1988); however, the distinction in relative side-chain distances between 3_{10}-helix and α-helix persists.

The ESR spectra for the 3K peptides are shown in Figure 3. The 3K-(4,7) and 3K-(4,8) spectra, which were reported earlier, show preferential broadening for the 3K-(4,7). This broadening arises from a distance-dependent spin–spin interaction between the labeled side chains (which will be discussed further below) and therefore demonstrates that on average $d(i,i+3) < d(i,i+4)$. Closer to the C-terminus, the 3K-(9,12) and 3K-(9,13) spectra are more similar to each other than are the 3K-(4,7) and 3K-(4,8) spectra, and both are sharper than the 3K(4,7). However, the relative broadening still indicates $d(9,12) < d(9,13)$.

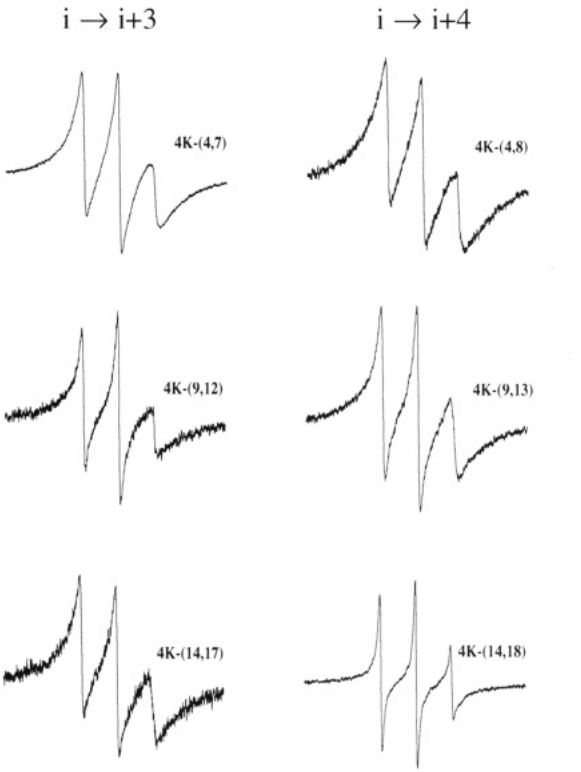

FIGURE 4: Continuous wave ESR spectra (100-G scan) of the 4K double-labeled peptides at 1 °C and peptide concentrations of 0.5–1.8 mM in 5 mM MOPS buffer, pH 7.1. The progression of the spin-label pairs through the helix is from the N-terminus (top spectra), to the center of the helix (middle spectra), and then to the C-terminus (bottom spectra).

The spectra of the 4K doubly labeled peptides are shown in Figure 4. In stark contrast to the results from the 3K peptides, the 4K-(4,7) and 4K-(4,8) spectra now both show substantial broadening, indicating $d(i,i+3) \geq d(i,i+4)$. This is a clear signature of α-helix near the N-terminus. The 4K-(9,12) and 4K-(9,13) report on the geometry in the middle of the 21-mer helix, and the spectra from these peptides are sharper than that found at the N-terminal region. These spectra still show that $d(i,i+3) \geq d(i,i+4)$, and it is apparent that, from the N-terminus to at least position 13, the 21-mer is largely α-helix. Interestingly, the final pair of spectra shows a reversal of the α-helix trend with the C-terminus giving $d(i,i+3) < d(i,i+4)$.

Peptides helices always contain a fraction of random coil. Therefore, it is important to determine how this random coil component impacts the ESR spectra. To explore this, we use guanidine hydrochloride (Gu·HCl), which readily unfolds peptide helices as determined by CD. Representative ESR spectra are shown in Figure 5 for two pairs of doubly labeled peptides in 8 M Gu·HCl. All of the spectra shown are nearly equivalent and only slightly broader than singly labeled peptide (monoradical) spectra. The broad features of the biradical spectra found for many of the peptides under helix-forming conditions (Figures 3 and 4) are clearly not observed. We find this to be the case for all the doubly labeled peptides. We conclude that an admixture of random coil and α-helix cannot be responsible for the different $i \rightarrow i+3$ and $i \rightarrow i+4$ distances observed throughout the 3K peptide and the C-terminus of the 4K peptide.

The theory of biradical nitroxides is well established (Atherton, 1973; Berliner, 1976). The strength of the biradical interaction is characterized by the exchange integral J, which measures the through-space overlap of the unpaired nitroxide

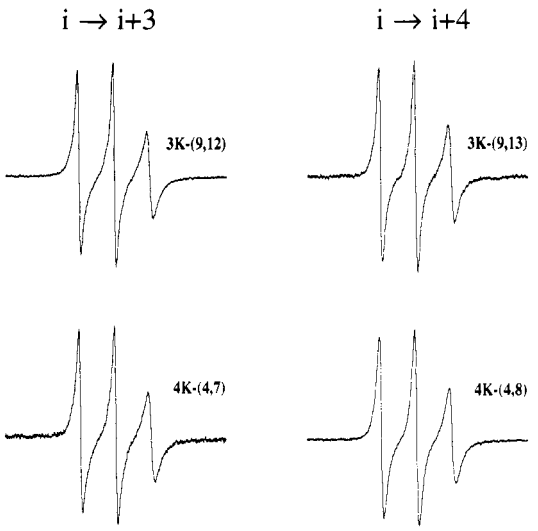

FIGURE 5: Continuous wave ESR spectra (100-G scan) of two 3K (top) and two 4K (bottom) double-labeled peptides at 22 °C in 8 M Gu·HCl. These denaturing conditions remove the spectral broadening associated with the helical structures.

electron orbitals. In general

$$J \approx J_0 \exp(-\beta r) \quad (1)$$

where r is the distance between radicals and β is the reciprocal of the length scale of the biradical interaction (Closs et al., 1992). This exponential dependence of r means that biradical spectra are very sensitive to the distance between nitroxide spins. It is interesting to note that J in NMR spectroscopy is limited to through-bond interactions whereas in ESR both through-bond and through-space couplings exist. In the peptides studied here, there are a sufficient number of covalent bonds designed into the molecular architecture to eliminate the through-bond contribution. This was demonstrated in previous work where an $i \rightarrow i+2$ doubly labeled peptide gave a weaker biradical interaction than $i \rightarrow i+3$ under helix-forming conditions.

When $J > 0$, each hyperfine line is composed of so-called singlet and triplet transitions. For small J, the singlet transitions form satellite lines next to the nitroxide hyperfine lines and exhibit transition frequencies that strongly depend on J (Glarum & Marshall, 1967). The outermost satellites split away from the outside +1 and −1 hyperfine lines (indicating the nitrogen nuclear spin states) to lower and higher field, respectively, with a separation of δ. When $J < a$, δ is related to J according to

$$\delta \approx J/2 + J^2/4a \quad (2)$$

where a is the hyperfine frequency (i.e., two times the separation between the +1 and −1 hyperfine lines) of 16.06 G. [Equation 2 is readily derived by considering the small J expansion of eq 2 in Glarum and Marshall (1967).] When J is small (i.e., $J \ll a$), these nearby satellite singlet transitions broaden the hyperfine lines. The low-field +1 line is the more narrow outside line and is therefore very susceptible to this broadening mechanism.

Shown in Figure 6 are several examples of simulated spectra with values of J from 0 to 4 G. The broadening of the +1 hyperfine line as J increases is apparent. Using reported values for the parameters in eq 1, from experiments with organic biradicals (Closs et al., 1992), a J value of 4.0 G corresponds to an approximate distance of 12.0 Å between the nitroxide spins. This is close to the expected distance between side chains under helix-forming conditions.

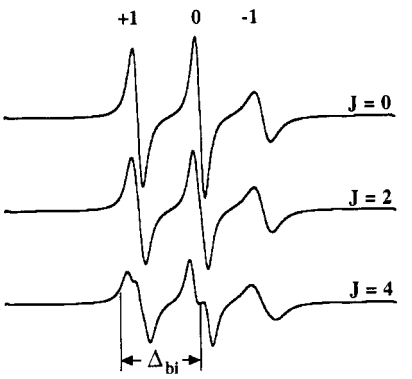

FIGURE 6: Simulated ESR spectra showing the biradical spectral broadening as the exchange integral, J (in G), is increased. Δ_{bi} is defined as the distance from the middle of the spectrum to the outside width at half-height of the +1 hyperfine line. Δ_{mono} is determined from a monoradical (singly labeled) peptide, and $|\Delta_{bi} - \Delta_{mono}|$ provides an estimate of the spectral broadening due to side-chain interactions.

Table II: Summary of the Biradical Line Broadening[a]

		$\lvert\Delta_{bi} - \Delta_{mono}\rvert$ (G)		
	x	$i \rightarrow i+3$	x	$i \rightarrow i+4$
3K-(4,x)	7	3.57	8	0.34
3K-(9,x)	12	1.86	13	0.86
4K-(4,x)	7	3.85	8	6.29
4K-(9,x)	12	2.00	13	2.43
4K-(14,x)	17	4.57	18	0.00

[a] All values were determined from spectra at 1 °C with peptide concentrations of 0.5–1.8 mM in 5 mM MOPS buffer, pH 7.1. Larger $|\Delta_{bi} - \Delta_{mono}|$ (see Figure 6) indicates a closer side-chain proximity.

Details observed in the calculated spectra of Figure 6 are smoothed out in the experimental spectra because side-chain flexibility and flickering between peptide conformations result in a distribution of distances between labels for each peptide. Thus, direct simulation of the spectra would require assumptions about the corresponding distribution of J values in the ensemble of peptide structures. Instead, we define a parameter Δ_{bi}, which is measured from the center of the spectrum to the outside width at half-height of the +1 hyperfine line (see Figure 6). The magnitude of Δ_{bi} increases in proportion to the shift of the singlet transitions away from the +1 line. Δ_{mono} is the same parameter except determined from a monoradical peptide. Therefore, $|\Delta_{bi} - \Delta_{mono}|$ is an approximate measure of δ (eq 2) and provides an estimate of J. The length scale of the biradical interaction β^{-1} (eq 1) is estimated to be 0.94 Å in organic biradicals and provides a calibration for the experimental data below (Closs et al., 1992). A decrease in average distance between the labels of 0.94 Å increases δ by a ratio of approximately 2.8 (when $J^2/4a \ll J/2$), and $|\Delta_{bi} - \Delta_{mono}|$ increases correspondingly. (Although not included in the analysis here, there is also a dipolar interaction between the spins which does not yield frequency shifts but does slightly narrow the singlet transitions. This may contribute to the high positive phase of the first-derivative low-field line in the experimental spectra.)

Summarizing the analysis above, $|\Delta_{bi} - \Delta_{mono}|$ measures the broadening of the +1 hyperfine line in the experimental spectra and increases in proportion to the average J. This parameter serves as a reliable and convenient method for ranking the spectra according to J. Δ_{bi} was measured for each peptide, and Δ_{mono} was measured from the singly labeled 3K-8 peptide (Miick et al., 1991). The results, $|\Delta_{bi} - \Delta_{mono}|$, are summarized in Table II. A pictorial representation of these data is shown in Figure 7. Bars of height $|\Delta_{bi} - \Delta_{mono}|$ are plotted between

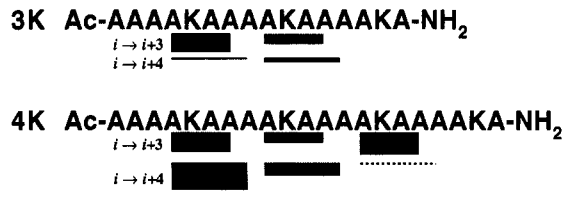

FIGURE 7: Pictorial representation of the spin-label side-chain interactions in specific regions of the 3K and 4K peptides. The heights of the bars below the sequences are proportional to the amount of spectral broadening ($|\Delta_{bi} - \Delta_{mono}|$) observed in the ESR spectra and inversely proportional to the distance between the indicated side chains. The dashed line indicates no detectable broadening.

double-label positions, indicating the relative spatial proximity of the labeled side chains under helix-forming conditions. Thicker bars indicate stronger interaction and closer side-chain proximity.

The 3K peptide shows weak $i \rightarrow i+4$ interactions relative to $i \rightarrow i+3$ (Figure 7) throughout its sequence, and this is evidence for 3_{10}-helix. The interactions closer to the C-terminus give a weaker $i \rightarrow i+3$ signal and may indicate more random coil in this region of the peptide. This is consistent with NMR findings on salt-bridged peptides (Liff et al., 1991) and recent measurements of helix dynamics in the 3K peptide that showed the C-terminus to be more dynamically frayed than the N-terminus (Miick et al., 1993). The 21-residue 4K reveals a very different story. Here the $i \rightarrow i+4$ interactions are equal to or stronger than the $i \rightarrow i+3$ from the N-terminus to position 13, and this is the expected signature of α-helix. The N-terminus gives the strongest interactions. The somewhat weaker interactions found in the middle of the peptide may indicate contributions from random coil. In contrast, the C-terminus exhibits the 3_{10}-helix signature, similar to that found in the 3K peptide, and demonstrates that the α-helix structure does not persist throughout the peptide. It is noteworthy that protein α-helices often have 3_{10}-helix distortions at their C-termini (Baker & Hubbard, 1984), and the results here suggest that this may be an intrinsic characteristic of general α-helix structure.

In Figure 7, the most profound difference observed between the 3K and the 4K peptides is at the N-terminus. The $i \rightarrow i+3$ interaction is very strong and nearly equal in the two peptides. Indeed, $d(i,i+3)$ is approximately the same for both 3_{10}-helix and α-helix. However, the $i \rightarrow i+4$ interaction clearly reveals a difference. This cannot be attributed to nitroxide side-chain flexibility or to specific interactions of the labels with other side chains or the helix termini; the labeling scheme (i.e., $4 \rightarrow 7$ and $4 \rightarrow 8$) and the N-terminal sequence in both the 3K and 4K peptides are exactly the same. The difference in the strength of the $i \rightarrow i+4$ interaction must reflect different helix geometry. We cannot rule out the possibility that the spin labels slightly influence the 3_{10}-helix $\rightarrow$ α-helix equilibrium. However, past work has shown that the MTSSL side chain rarely influences secondary structure in either peptides (Todd & Millhauser, 1991) or proteins (Altenbach et al., 1990). Further, the results of the 4K compare favorably with recent NMR work which demonstrated α-helix geometry for the N-terminus of a similar 21-residue peptide (Lockhart & Kim, 1993).

The 3K peptide probably exists as a mixture of 3_{10}-helix and α-helix, and further experiments will be required to resolve the relative proportions. The sharp spectra observed for the 3K-(4,8), for example, may contain broad low-amplitude contributions from α-helix. The sharper lines expected for 3_{10}-helix can dominate the shape of the ESR spectrum, but a broad component may represent a comparable proportion of α-helix. Nevertheless, by comparing the N-termini of the 3K and 4K peptides, we conclude that there is clearly a significant contribution from 3_{10}-helix in the shorter sequence.

The results presented here reveal a remarkable similarity to those from $(\text{Aib-L-Ala})_n$ sequences which exhibit a length-dependent $3_{10} \rightarrow \alpha$-helix transition (Pavone et al., 1990). For $n = 3$ this sequence is completely 3_{10}-helix whereas for $n = 4$ the geometry is mostly α-helix with two 3_{10}-helix hydrogen bonds. Such a transition clearly demonstrates that C_α-monosubstituted amino acids, such as Ala, are strained in the 3_{10}-helix geometry. Increasing peptide length increases this strain to the point where α-helix becomes the favored conformation. The findings presented here suggest that peptides without Aib also exhibit characteristics of a $3_{10} \rightarrow \alpha$ transition although for much longer peptide sequences. At this time it is not clear why 3_{10}-helix is significantly populated in the shorter 16-residue sequences. Theoretical studies have indicated that increased hydrogen bonding and conformation-dependent electrostatics may play a role (Hodgkin et al., 1990). For example, in completely ordered helices of fixed sequence length, 3_{10}-helix forms one more hydrogen bond than α-helix. One can speculate that, even in significantly frayed helices, the 3_{10} geometry benefits energetically from the formation of an additional helix hydrogen bond. Further, the more open 3_{10} structure may increase favorable contacts of the main-chain hydrogen bonds with the aqueous solvent (Tirado-Rives et al., 1993). Other factors to consider are the quantity and placement of the charged Lys^+ residues since they are more helix destabilizing than Ala. In the future work it will be interesting to probe the sequence dependence of the 3_{10}-helix $\rightarrow$ α-helix transition.

ACKNOWLEDGMENT

We thank Dr. J. Handey for helpful thoughts and discussion.

REFERENCES

Altenbach, C., Marti, T., Khorana, H. G., & Hubbell, W. L. (1990) *Science 248*, 1088–1092.

Atherton, N. M. (1973) *Electron Spin Resonance: Theory and Applications*, Wiley, New York.

Baker, E. N., & Hubbard, R. E. (1984) *Prog. Biophys. Mol. Biol. 44*, 97–179.

Barlow, D. J., & Thornton, J. M. (1988) *J. Mol. Biol. 201*, 601–619.

Berliner, L. J., Ed. (1976) *Spin Labeling: Theory and Applications, Molecular Biology*, Academic Press, New York.

Berliner, L. J., Grunwald, J., Hankovsky, H. O., & Hideg, K. (1982) *Anal. Biochem. 119*, 450–455.

Chakrabartty, A., Kortemme, T., Padmanabhan, S., & Baldwin, R. L. (1993) *Biochemistry 32*, 5560–5565.

Closs, G. L., Forbes, M. D. E., & Piotrowiak, P. (1992) *J. Am. Chem. Soc. 114*, 3285–3294.

Creamer, T. P., & Rose, G. D. (1992) *Proc. Natl. Acad. Sci. U.S.A. 89*, 5937–5941.

Forester, A. R., Hay, J. M., & Thomson, R. H. (1968) *Organic Chemistry of Stable Free Radicals*, Academic Press, New York.

Glarum, S. H., & Marshall, J. H. (1967) *J. Chem. Phys. 47*, 1374–1378.

Hodgkin, E. E., Clark, J. D., Miller, K. R., & Marshall, G. R. (1990) *Biopolymers 30*, 533–546.

Kemp, D. S., Boyd, J. G., & Muendel, C. C. (1991) *Nature 352*, 451–454.

Liff, M. I., Lyu, P. C., & Kallenbach, N. R. (1991) *J. Am. Chem. Soc. 113*, 1014–1019.

Lockhart, D. J., & Kim, P. S. (1993) *Science 260*, 198–202.

Luckhurst, G. R., & Pedulli, G. F. (1971) *Mol. Phys. 20*, 1043–1055.
Lyu, P. C., Liff, M. I., Marky, L. A., & Kallenbach, N. R. (1990) *Science 250*, 669–673.
Marqusee, S., Robbins, V. H., & Baldwin, R. L. (1989) *Proc. Natl. Acad. Sci. U.S.A. 86*, 5286–5290.
Mertuka, G., Shalongo, W., & Stellwagen, E. (1991) *Biochemistry 30*, 4245–4248.
Miick, S. M., Todd, A. P., & Millhauser, G. L. (1991) *Biochemistry 30*, 9498–9503.
Osterhout, J., Jr., Baldwin, R. L., York, E. J., Stewart, J. M., Dyson, H. J., & Wright, P. E. (1989) *Biochemistry 28*, 7059–7064.
Miick, S. M., Martinez, G. V., Fiori, W. R., Todd, A. P., & Millhauser, G. L. (1992) *Nature 359*, 653–655.
Miick, S. M., Casteel, K. M., & Millhauser, G. L. (1993) *Biochemistry 32*, 8014–8021.
Pavone, V., Benedetti, E., Diblasio, B., Pedone, C., Santini, A., Bavoso, A., Toniolo, C., Crisma, M., & Sartore, L. (1990) *J. Biomol. Struct. Dyn. 7*, 1321–1331.
Scholtz, J. M., & Baldwin, R. L. (1992) in *Annual Review of Biophysics and Biomolecular Structure* (Engelman, D. M., Cantor, C. R., & Pollard, T. D., Eds.) pp 95–118, Annual Reviews Inc., Palo Alto, CA.
Schultz, G. E., & Schirmer, R. H. (1979) *Principles of Protein Structure*, Springer-Verlag, New York.
Tirado-Rives, Maxwell, & Jorgensen (1993) *J. Am. Chem. Soc.* (in press).
Todd, A. P., & Millhauser, G. L. (1991) *Biochemistry 30*, 5515–5523.
Toniolo, C., & Benedetti, E. (1991) *Trends Biochem. Sci. 16*, 350–353.
Vila, J., Williams, R. L., Grant, J. A., Wojcik, J., & Scheraga, H. A. (1992) *Proc. Natl. Acad. Sci. U.S.A. 89*, 7821–7825.